Modeling for proximate analysis and heating value of torrefied biomass with vibration spectroscopy

Brian K. Via[*,a,b,c,], Sushil Adhikari[b,c], Steve Taylor[b,c]

a *Forest Products Development Center, School of Forestry and Wildlife Sciences, Auburn University, Auburn, AL 36849, USA*

b *Department of Biosystems Engineering, Auburn University, Auburn, AL 36849, USA*

c *Center for Bioenergy and Bioproducts, Auburn University, Auburn, AL 36849, USA*

Note: This is the Accepted Author Manuscript Version for the following Journal Publication Reference below.

Via, B. K., Adhikari, S., & Taylor, S. (2013). Modeling for proximate analysis and heating value of torrefied biomass with vibration spectroscopy. Bioresource technology. 133: 1–8.

[*] Corresponding author at: Forest Products Development Center, School of Forestry and Wildlife Sciences, Auburn University, 520 Devall Drive, Auburn University, Alabama 36849
E-mail address: bkv0003@auburn.edu (B. Via), Telephone: 334-844-1088 and Fax: 334-844-1084

Abstract

The goal of this study was to characterize the changes in biomass with torrefaction for near infrared reflectance (NIR) and attenuated total reflectance Fourier transform infrared (ATR-FTIR) spectroscopy for sweetgum, loblolly pine, and switchgrass. Calibration models were built for the prediction of proximate analysis after torrefaction. Two dimensional (2D) correlation spectroscopy between NIR and FTIR was found to precisely explain the depolymerization at key functional groups located within hemicellulose, cellulose, and lignin. This novel 2D technique also demonstrated the possibility of assigning key NIR wavenumbers based on mid IR spectra. Hemicellulose based wavenumbers were found to be most sensitive to torrefaction severity with complete degradation at 250-275^{o}C. Lignin associated wavenumbers exhibited the least degradation to severity but was still detected with 2D correlation spectroscopy. Finally, calibration models for proximate analysis were performed and while both systems could be used for rapid monitoring, NIR performed better than FTIR.

Keywords: near infrared, mid infrared, torrefaction, biomass, proximate

1. Introduction

Conversion of biomass into energy is an attractive alternative to petroleum based oil as the international community looks to lower carbon dioxide (CO_2) emissions that are not part of the natural renewable cycle. However, conversion of biomass into bioenergy presents several hurdles when compared to petroleum including a lower calorific value and higher moisture content due to the hygroscopic nature of biomass. Torrefaction of biomass is one solution to increasing the energy content which is attributable to the reduction in hemicellulose content after treating at temperatures in the range of 200^{o}C to 300^{o}C. Another advantage of torrefied biomass is the increased hydrophobicity which is due to the degradation of hemicellulose at high temperatures which previously allowed for significant moisture sorption because of amorphous structure and consequent availability of OH groups of the native hemicellulosic structure (Olsson and Salmen, 2004). The torrefaction also targets the amorphous region of cellulose at 270 to 300^{o}C which further improves the resistance of the feedstock to moisture sorption. Because lignin is fairly resistant at temperatures below 300^{o}C, what is left is a higher concentration of lignin which results in a hydrophobic torrefied biomass (Ehara et al., 2002).

It is also anticipated that the degradation of hemicellulose will improve the uniformity of the biomass feedstock. However, because lignin is stable and remains for higher energy conversion, there are still many phenolic type compounds within the biomass and between biomass sources (Ralph and Hatfield, 1991). This variation in the remaining polymer structure after torrefaction will need to be monitored so that processing parameters can be adjusted

accordingly. Rapid techniques to monitor feedstock quality would be useful but should require minimal sample preparation and low cost of analysis.

Near infrared reflectance (NIR) and Fourier transform infrared (FTIR) spectroscopy are two vibration based techniques that can rapidly measure the spectra which is associated with the key functional groups within the biopolymers. NIR has been shown to be faster and more precise in the prediction of biomass density than FTIR while multivariate models from both techniques relied on the vibration of key functional groups (Via et al., 2011). It is this key relationship between wood chemistry and spectra that allows for the development of multivariate calibration equations for FTIR and NIR. Recently NIR has shown promise in the characterization of torrefied wood to monitor the shift in biomass quality with temperature and duration (Rousset et al., 2011b) and has been shown to be sensitive to heat pretreatments as low as 121 ^{o}C (Huang et al., 2013).

Still, it would be useful to monitor key process metrics that are traditionally obtained through time consuming and proximate analysis such as moisture, ash, volatile matter, fixed carbon and higher heating value (HHV). But torrefaction will apply heat and duration treatments that will degrade or modify the fundamental chemistry. Application of these analytical tools to this scenario would also be useful. Labbe et al. was able to trace the disappearance of key functional groups in the mid infrared region as wood-derived-charcoal was heated to 350^{o}C (Labbe et al., 2006). This work also proved fruitful in that they condensed the spectra into principal components and was able to successfully partition the biomass by thermal treatment while the loadings within the PC was utilized to identify important

wavenumbers. Likewise, NIR has been utilized to characterize the biomass with increases in temperature. For example, when wood was exposed to 220^{o}C for 4 hours, it was found that there were changes in the spectra related to the change in OH, CH, CH_2, and CH_3 overtone vibrations (Schwanninger et al., 2004).

Because of the sensitivity of NIR and FTIR spectra to changes in temperature, duration of exposure, and the consequent change in functional groups, it is hypothesized that accurate and precise multivariate models can be built for important proximate analysis metrics that may be related to these functional groups. Proximate analysis and HHV will be measured using standard techniques and multivariate models from FTIR and NIR spectra will be built. Furthermore, the assignment of functional groups in the near infrared domain as given in the literature (Schwanninger et al., 2011) will be confirmed through two dimensional (2D) correlation analyses with FTIR spectroscopy. This 2D technique has been shown to be a powerful analytical tool that can partition and explain the relationship between the spectra in the NIR and mid infrared region for subtle changes in cellulose, hemicellulose, and lignin content (Barton et al., 1992). Because temperature modification is more extreme than subtle changes in wood chemistry, it is anticipated that 2D correlation spectroscopy should accurately identify and assign wavelengths in the NIR region based on strong correlations to the mid infrared region. The goal of this study was to characterize the changes in biomass with torrefaction for near infrared reflectance (NIR) and attenuated total reflectance Fourier transform infrared (ATR-FTIR) spectroscopy for sweetgum, loblolly pine, and switchgrass. Multivariate models and 2D correlation spectroscopy will be utilized to better under the sequence of depolymerization with thermal exposure.

2. Methods

2.1 Materials, Heat Treatment and Experimental Design

Detailed procedure for sample preparation and torrefaction of biomass samples can be found elsewhere (Carter, 2012). Briefly, loblolly pine (*Pinus taeda*), sweetgum (*Liquidambar styraciflua*) and switchgrass (*Panicum virgatum*) were acquired from the Research Station at Auburn University. Loblolly is the most commercially important softwood in the southern United States and was chosen as the most likely conifer feedstock. Sweetgum was chosen because it is an underutilized but fast growing hardwood in the same geographical region as loblolly. Finally, switchgrass was chosen due to its north-south range and ecological dominance. Each of the three biomass types was treated at three temperatures and three times, and the experimental design utilized for calibration can be observed in Table 1. At the end of the treatment time, the biomass samples were pulled from the furnace and immediately placed in desiccators for characterization.

2.2 Biomass Characterization

Moisture content of each sample was found using an Ohaus moisture analyzer (model MB45, Parsippany, NJ). Ash content was found according to NREL (web reference). For volatile matter determination, samples were shipped to Hazen Research Laboratory (Golden, CO) for analysis using ASTM D3175-11. Fixed carbon (FC) of the samples was determined indirectly according to the Eqn. 1

$$FC\% = 100\% - ash_{dry}\% - volatile\% \quad (1)$$

The energy content of the biomass was measured with a bomb calorimeter (IKA Works Inc. Model C200, Wilmington, NC). Average values were reported based on three measurements.

2.3 Vibration Spectroscopy

Mid -IR spectra were collected between 4000 and 650 cm^{-1} using a PerkinElmer Spectrum model 400 (Perkin Elmer Co., Waltham, MA). This equipment utilized a single reflectance ATR diamond with a repeatable vertical pressure between samples to ensure repeatability in spectra acquisition between samples. Within a sample, the spectra was collected within 10 seconds of applying the vertical load since relaxation of the polymer can occur over time resulting in decreased absorbance of the mid infrared spectra. The ATR diamond was cleaned with acetone prior to data collection. All scans were carried out at room temperature which was approximately $22^{o}C \pm 1$. Even though the samples were torrefied, care was taken to replicate the time out of the sample to minimize error due to moisture pickup.

The NIR spectra were acquired between 10000 to 4000 cm^{-1} wavenumbers. Wavenumbers were utilized in preference over wavelengths so that NIR and Mid-IR could be compared utilizing the same units. The same PerkinElmer Spectrum model 400 (as mid IR) was utilized to capture the NIR but with an NIR module. The sample window (0.8 cm) was cleaned with acetone prior to spectra collection. All scans were performed at 4 nm resolution and a single scan consisted of an average of eight scans from the same position. A reference check was run every 20 minutes using a Spectralon standard.

2.4 Chemometric Analysis

To facilitate NIR modeling in the statistical analysis software (SAS) package, the spectra in the near infrared region was reduced to 10 nm intervals prior to the conversion to wavenumbers; likewise, the mid infrared region was also reduced to 10 cm^{-1} interval because the SAS software was likewise unable to process larger data matrixes (Via et al., 2011). This procedure was found to allow for data analysis of large data matrixes without degradation of calibration equations (Via et al., 2011). The spectra was then adjusted to a mean =0 and a standard deviation =1 to allow for equal comparison of loadings across different wavenumbers. In addition to the native spectra, the 1st derivative was computed to remove baseline shifts and was calculated as the slope between two adjacent points across the entire wavenumber range.

The spectra in the IR and NIR range was then reduced to principal components as defined in Eqn. 2 and 3.

$$PC_1 = C_{11}W_1 + C_{12}W_2 + \ldots C_{1j}W_j \quad (2)$$

$$PC_2 = C_{21}W_1 + C_{22}W_2 + \ldots C_{2j}W_j \quad (3)$$

In which the coefficient C represents the loading or weight of the linear combination equation at W_j and W represents the absorbance at the j^{th} wavenumber. PC_1 represents the dimension in the data matrix with the largest source of variation, PC_2 accounts for the second largest source of variation, and PC_{last} (the last PC) accounts for the dimension with the smallest source of variation. However, during analysis, the top 10 PC's accounted for > 99% of the overall variation for both NIR and FTIR and thus the total factors/PC's for analysis were restricted to a maximum of 10. Wavenumbers with high absolute coefficients |C| represent a higher influence on that dimension. This procedure (Eqn. 2-3) was repeated for each PC in which the

number of factors (PC's) equals the number of wavelengths (j) although only the top 10 PC's were retained for modeling. The algorithm sets the following scaled conditions when computing C_{ij} (Eqn. 4):

$$C_{11}^2 + C_{12}^2 + \ldots. C_{ij}^2 = 1 \qquad (4)$$

And the covariance matrix **S** can be defined as

$$\mathbf{S} = 1/(n-1)W'W \qquad (5)$$

in which the PC's are the eigenvectors of the covariance matrix of the absorbance's that make up the spectra and the variances along each dimension are the eigenvalues of **S**. For a more detailed discussion on these equation derivations, please refer to Cowe and McNicole (1985).

Then principal components regression (PCR) models were computed using standard multiple linear regression routines in SAS and following the Full Eqn. 6.

$$Y = C_1PC_1 + C_2PC_2 + \ldots..+ C_iPC_{i+} e_i \qquad (6)$$

In which e is the random error and Y is the proximate analysis metric of interest. Eqn. 6 was shortened to a reduced model in which only C_iPC_i combinations with a p-value of the slope < 0.05 were retained for prediction of the metric Y.

Regression diagnostics were analyzed to determine which calibration models were the most robust, accurate, and precise. These diagnostics included root mean square error for calibration (RMSEC), R^2, and adjusted R^2. For model cross validation, the predicted sum of squares (PRESS) error was calculated and converted to a RMSEP following the equations given

in (Casal et al., 1996). The RMSEP was plotted against the number of PC's (not shown) to determine the cut-off point between too many and too few parameters. Selection of too few parameters results in models that only provide a rough approximation of the experimental data while selection of too many variables results in overfit. Overfit is a common problem in which too many variables are added to the model which inflates the apparent performance during calibration but performs poorly when new samples are measured. The backward selection method was used to determine which principal components were necessary for prediction of the independent variables (proximate analysis). Additionally , a p-value criteria < 0.05 was set for variable selection to ensure that the reduced model from Eqn. 6 did not futher result in overfit.

3. Result and Discussion

3.1 Proximate analysis and heating value

Table 2 shows the results for proximate analysis of the samples. Ash and fixed carbon contents of the treated samples increased while volatiles decreased as the temperature and time of treatment increased. At the most intense treatment conditions, each biomass type showed a decrease in volatile content of up to ~50%, while ash percentages approximately doubled, and fixed carbon percentages tripled. Only volatile matters are driven off the biomass during torrefaction, leaving the ash and fixed carbon portions. These trends agree with other studies of torrefied biomass (Prins et al., 2006).

3.2 NIR spectral response

Between 10,000 and 7,000 cm^{-1}, a lower baseline shift was observed when transitioning from the control to 225^{o}C and this was in spite of the slightly darker color in the samples (spectra not shown). A similar observation was observed for sweetgum and switchgrass. Color changes were observed from darker brown at lower temperatures to nearly black at 300^{o}C. This agrees with Deng et al. who observed only a mild brown color at lower torrefaction temperatures but black for samples treated at 300^{o}C. It is theorized that the downward shift in spectra at 225^{o}C may be attributable to the degradation of hemicellulose that occurs around that temperature resulting in lower densities of the individual particles. With lower density, the absorbance will decrease as a function of lower concentrations of these amorphous structures. At this temperature, cellulose has been shown to show considerable resistance to thermal cleavage of the polymer while hemicellulose degradation is just beginning. For example, at 230^{o}C only 3% of the hemicellulose was consumed for hemicellulose that was extracted from bagasse and processed with thermal gravimetric analysis (Chen and Kuo, 2011a).

Given the complex baseline shift in spectra with thermal degradation that was observed, the first derivative was applied to increase the sensitivity of key peaks with increases in temperature (pretreated spectra not shown). Conversion of the spectra to the first derivative after torrefaction will help to improve the precision of the peaks that may not be seen in the native spectra due to broad overlapping peaks that are common in the near infrared region (Rousset et al., 2011b). The wavelength 5220-5051cm^{-1} has been shown to be related to the O-H stretch and deformation in water and was sensitive to torrefaction in this study; however, it should be pointed out that dehydration of free and then bound water occurs well below the temperatures in this study. As such, the degradation of wavelengths between 5220-5051 cm^{-1} is

probably attributable to the reduction in O-H groups that occurs during torrefaction. This was observed for torrefied beach in which the same wavelength range diminished as the temperature increased coupled with 8 hour duration (Rousset et al., 2011b).

The wavenumber at 7410, 6003, and 5848 cm^{-1} were sensitive to temperature increases and can be associated with hemicellulose degradation. The wavenumber 7410 cm^{-1} appeared most sensitive to temperature increases particularly at temperatures equal to or greater than 250^{o}C. This was attributable to the disappearance of CH and CH_3 functional groups associated with hemicellulose (Phanphanich and Mani, 2011; Schwanninger et al., 2011). The degradation of CH_3 was probably associated with the cleavage of acetyl groups in hemicellulose during temperature increases which has been shown to be the first to depolymerize under higher temperatures (Tjeerdsma and Militz, 2005). There was also an apparent degredation at 7080 cm^{-1} and this may have been attributable to the degradation of O-H bonds in water molecules (Schwanninger et al., 2011).

At 15 minutes duration, there was not much depolymerization of cellulose as indicated by the wavenumbers at 6660, 5464, and 4370 cm^{-1} which was attributable to the O-H, C-O, and C-H vibrations in cellulose. However, when longer durations were exposed to the biomass, these wavelengths began to also degrade particularly at higher temperatures. Conversely for lignin, as indicated by the lack of degradation of the C-H stretch for aromatic portions of lignin (5980 cm^{-1}), the lignin based polymer was resistant to thermal depolymerization during torrefaction. This was expected as lignin at best only experiences mild depolymerization at temperatures tested in this study but typically longer exposure times are required (Shang et al., 2012). This

was indicative of the torrefaction of bamboo in which the concentration of lignin actually increased at 280^{o}C based on mid infrared spectra and this was attributed to the resistance of the β-O-4 bond to thermal decomposition (Rousset et al., 2011a).

3.3 NIR versus FTIR two dimensional correlation spectroscopy

The experimental design in this study allowed for the external perturbation of temperature and duration on biomass modification which can then be simultaneously monitored with NIR and FTIR. Two dimensional (2D) correlation methodologies allow for the interpretation of changes in the modification of the biomass as temperature or duration increases. The correlation of combination and overtone bands in the NIR can then be associated with fundamental vibrations from FTIR. Fig. 1 represents a slice of the NIR versus FTIR in which there is significant correlation via the pearson correlation coefficient. Other graphs were generated (not shown) and the important correlations were summarized in Table 3. Because of the overtone and combination bands in the NIR, there were often wide regions that exhibited significant correlation making it more difficult to partition out true peaks. As such, application of the first derivative prior to 2D analysis was found to be partially helpful in resolving the peaks in the NIR and mid-IR region (Fig. 1). Also, the lower r-value regions in the graph had to be filtered out and the higher r-value categories were widened to 0.4-0.6 (medium correlation) and 0.6 to 0.8 (high correlation) such that only relevant chemical information could be extracted from the analysis.

Significant correlations from the red zones in Fig. 1 and similar graphs (not shown) were found to correspond closely when compared to peaks observed with torrefaction. The most

significant peaks from these red zones were then exported to Table 3 and the vibrations associated with temperature and duration increases were identified and band assignments were performed. It was not surprising that the highest correlation (r=0.84) was attributable to the high reactivity and degradation of hemicellulose at 5848 versus 1740 cm^{-1}. This was expected given that hemicellulose degradation begins before cellulose and lignin for the temperatures tested in this study. The significance of 5848 cm^{-1} was due to the C-H stretch in furanose or pyranose and this corresponded to 1740 cm^{-1} which was attributable to the C=O stretch in hemicellulose. This was observed in another study in which spruce wood was heated to 140^{o}C through steam for 5 to 100 hours and the response in the NIR region was monitored. They found significant effects of steam treatment on the C-H stretch due to pyranose and furanose degradation with time (Mitsui et al., 2008). Other significant correlations associated with hemicellulose occurred at 7414 and 6003 versus 1360 cm^{-1} due to the sensitivity of both regions to C-H bonds in hemicellulose.

Cellulose associated wavenumbers in the NIR region were found to correlate with torrefaction severity at 6660, 5464, and 4392 - 4365 cm^{-1} with the latter exhibiting the strongest correlation to FTIR spectroscopy (Table 3). The assignment at 4392-4365 cm^{-1} was attributable to the weak carbonyl (C=O) stretch in cellulose. This behavior can be explained by observations with CP/MAS ^{13}C NMR in which large concentrations of carbonyl groups were found in the torrefied residue due to the eradication of cellulose and hemicellulose for loblolly pine, which was one of the three species used in this study (Ben and Ragauskas, 2012).

Finally, lignin associated wavenumbers were found to be least resistant to thermal treatment both in the NIR and FTIR region. Nevertheless, significant correlations were found between FTIR and NIR region due to the C-H bond associated with the aromatic portion of the polymer (Table 3). These correlations were as high as r=0.77 and could partially be explained by the increase in signal clarity as other polymers diminish with temperature increases. Such difficulty in interpretation has been observed by others in which the covariance between functional groups of various polymers is high since multiple polymers will depolymerize and trend in sequence (Alciaturi et al., 2001). As such, while powerful, 2D correlation spectroscopy should be coupled with more traditional chemometric techniques to ensure proper analysis of the trends within the data analysis.

3.4 Calibration and prediction capability of NIR and FTIR

Table 4 demonstrates the ability to calibrate NIR and FTIR for proximate analysis of torrefied biomass. Both techniques proved useful in the rapid monitoring of these traits and could be easily implemented in quality control laboratories located at the manufacturing plant. All models required 5 to 8 factors depending on the pretreatment, spectroscopic method, and metric. In all cases, NIR performed slightly to considerably better than FTIR in both R^2 and RMSEP and on average, the same number of factors for prediction were necessary for both systems. Perhaps the better performance with NIR is to be expected because it has been shown to be superior in the calibration of biomass chemistry which should drive the variation in proximate analysis. This was observed for bamboo in which the holocellulose, α-cellulose, klason lignin, and extractives content were predicted better with NIR than FTIR (Sun et al., 2011). Additionally, Kelley et al. demonstrated good correlations of NIR based partial least

squares regression models to fundamental sugars for 15 different types of biomass (Kelley et al., 2004). As Table 3 indicates, it is the degradation (or lack thereof) of functional groups within lignin, cellulose, and hemicellulose that is most sensitive to torrefaction severity. Furthermore, the HHV has been shown to be nonlinearly associated to fixed carbon and volatiles and linearly related to lignin and ash (Demirbas, 2003). The interrelationship between HHV, other proximate analysis, and underlying chemistry helps to explain the successful calibration of models in this study although samples from future populations should be appended to the calibration model to ensure proper evolution of the model with time (Doublet et al., 2013).

The two best performing calibrations occurred with NIR based spectra to monitor the volatiles and fixed carbon both of which saw an adjusted R^2 of 0.98 (Table 4). Perhaps the superiority in the volatiles model can be attributed to the nature of torrefaction. As demonstrated in Table 3, the reactivity of the polymers varies with torrefaction severity resulting in the unzipping of polymers with hemicellulose exhibiting the most degradation and lignin exhibiting the least. Likewise, the fixed carbon is the residual carbon within the torrefied material that was not volatilized and this interrelationship may help to explain the similar predictability for fixed carbon as volatiles. Additionally, as Table 3 demonstrates, the advanced ability to predict fixed carbon perhaps should not be surprising given that most band assignments are either C-H or C-O.

The HHV and ash also exhibited strong calibrations with NIR with an adjusted R^2 of 0.91 (Fig. 2 a-e and Table 4). As discussed earlier, the HHV has complex interrelations with the chemistry,

ash, fixed carbon, and volatiles and this complexity could result in higher errors during model building resulting in a lower R^2, particularly when nonlinear relationships occur. Since PCR is a linear based model, any deviation from linearity will add to the predicted error. For ash, considerable deviation from linearity can be seen with the residuals around the 1:1 line starting low and ending low at the edges of the range of the distribution (Fig. 2b). A similar deviation from linearity was observed when predicting ash content for wood and herbaceous biomass (Labbé et al., 2008). In that work, they were only able to alleviate the nonlinearity when orthogonal signal correction (OSC) coupled with partial least squares (PLS) regression was used. Application of OSC prior to modeling helps to remove unwanted variation in the X matrix while PLS can further remove or alleviate deviation issues. However, this study elected not to pursue these types of preprocessing techniques but instead keep the data matrix closer to its native state which has been shown to assist in model interpretation (Hair et al., 2006) while PCR was chosen because classical statistical theory can be applied during model development. Instead, PLS is better utilized for prediction purposes albeit the advantage over PCR is much less than most researchers believe with other advantages including: a requirement of fewer latent variables, utilization of correlations with the y variable during score computation, and better resistance to nonlinear behavior (Wentzell and Montoto, 2003).

The moderately strong R^2 for ash agreed with other studies which included 20 non-torriefied feedstocks (Sanderson et al., 1996) and yellow poplar (Nkansah et al., 2010) but was much better than PLS-NIR models for *Miscanthus x giganteus* , which yielded only an R^2 of 0.58 (Fagan et al. 2011). The prediction of moisture was the worst performer with an adjusted R^2 of 0.84 and part of this error could be witnessed with the negative residuals at higher moisture levels

(Fig. 2c). This was probably attributable to the lower range of moisture that was observed after torrefaction which could have reduced the leverage available during model building. Additionally, it is probable that a model for moisture content using the simpler PCR method was not as strong as other studies which utilized PLS coupled with multiple spectra pretreatments (Fagan et al. 2011). Nevertheless, the predictability of the models using PCR were still strong with only minor deviations in linearity for most proximate metrics except moisture (Fig. 2). Further analysis (not shown) found that adding more factors in these PCR models would have reduced or resolved the non-linear issues; however, it could have resulted in overfit as indicated by only inappreciable RMSEP improvements.

Since 2D correlation analysis proved useful in identifying wavenumbers that were sensitive to changes in temperature and duration, the calibration models were further investigated to understand if severity of treatment had any effect on model development. To be consistent, the 1st derivative was applied for all comparisons to remove baseline variation. While many factors were often necessary to fully model the proximate analysis metrics (Table 4), PC_1 and PC_2 exhibited the most influence on all metrics and for both spectroscopy systems as determined by p-values < 0.0001 and suggests a common covariance between biomass chemistry and all of the proximate analysis metrics. As such, other factors (PC_3 – PC_{10}) with varying levels of coefficents (Eqn. 6) were often necessary to differentiate proximate analysis models. Despite PC_1 and PC_2 accounting for most of the systematic variance of the FTIR and NIR system (>70%), most of the wavenumbers with significant loadings were not associated with thermal treatments as exhibited in Table 3. Wavenumbers that were associated with treatment severity for FTIR based models were 1740 (PC2: C=O stretch hemicellulose), 1600

(PC_2: H_2O), and 850 cm^{-1} (PC_4: C-H stretch aromatic) while for NIR models the coefficient weights were high at 5464 ($PC_{3,4}$: O-H str. + C-O str. in cellulose) and 5980 (PC_4: C-H stretch aromatic) cm^{-1}. This suggests that multivariate models were somewhat reliant on treatment severity but 2D correlation spectroscopy was necessary to identify the suite of functional groups associated with thermal degradation.

4. Conclusions

The results demonstrated the ability of both spectroscopy techniques to monitor key proximate analysis metrics during torrefaction of switchgrass, loblolly pine, and sweetgum. NIR performed better than ATR-FTIR for most multivariate models. Fixed carbon and volatiles were the easiest to predict while ash and higher heating value was also well predicted after torrefaction. Two dimensional correlation spectroscopy proved to be a valuable technique in explaining key changes during polymer degradation of hemicellulose and cellulose. 2D correlation spectroscopy was also more sensitive to subtle changes in lignin than PCR modeling.

Acknowledgements

The authors would like to Mr. Chad Carter for preparing torrefied biomass and performing proximate analysis and heating value, and the Southeastern Sun Grant for funding this study. However, only the authors are responsible for the opinions expressed in this paper and for any remaining errors.

References

1. Alciaturi, C.E., Escobar, M.E., de La Cruz, C., Vallejo, R. 2001. Determination of chemical properties of pyrolysis products from coals by diffuse-reflectance infrared spectroscopy and partial least squares. *Analytica Chimica Acta*, **436**(2), 265-272.
2. Barton, F.E., Himmelsbach, D.S., Duckworth, J.H., Smith, M.J. 1992. 2-Dimensional Vibration Spectroscopy - Correlation of Midinfrared and near-Infrared Regions. *Applied Spectroscopy*, **46**(3), 420-429.
3. Ben, H.X., Ragauskas, A.J. 2012. Torrefaction of Loblolly pine. *Green Chemistry*, **14**(1), 72-76.
4. Carter, C. 2012. Physicochemical properties and thermal decomposition of torrefied woody biomass and energy crop. M.S. Thesis (unpublished), Auburn University, Auburn, AL.
5. Casal, V., MartinAlvarez, P.J., Herraiz, T. 1996. Comparative prediction of the retention behaviour of small peptides in several reversed-phase high-performance liquid chromatography columns by using partial least squares and multiple linear regression. *Analytica Chimica Acta*, **326**(1-3), 77-84.
6. Chen, W.H., Kuo, P.C. 2011a. Isothermal torrefaction kinetics of hemicellulose, cellulose, lignin and xylan using thermogravimetric analysis. *Energy*, **36**(11), 6451-6460.
7. Cowe, I.A., McNicole, J.W. 1985. The Use of Principal Components in the Analysis of Near-Infrared Spectra. *Applied Spectroscopy,* **39**(2), 257-266.
8. Demirbas, A. 2003. Relationships between heating value and lignin, fixed carbon, and volatile material contents of shells from biomass products. *Energy Sources*, **25**(7), 629-635.
9. Doublet, J. 2013. Predicting the biochemical methane potential of wide range of organic substrates by near infrared spectroscopy. *Bioresource Technology*, **128**(1), 9-17.
10. Ehara, K., Saka, S., Kawamoto, H. 2002. Characterization of the lignin-derived products from wood as treated in supercritical water. *Journal of Wood Science*, **48**(4), 320-325.
11. Fagan, C., Everard, C., McDonnell, K., 2011. Prediction of moisture, calorific value and carbon content of two dedicated bioenergy crops using near-infrared spectroscopy. *Bioresource Technology*, **102**(8), 5200-5206.
12. Hair, J., Black, W., Babin, B., Anderson, R., 2006. Multivariate Data Analysis, 7th ed. Upper Saddle River, New Jersey.
13. Huang, J., Xia, T., Li, A., Yu, B., Qing, L., Tu, Y., Zhang, W., Yi, Z., Peng, L. 2012. A rapid and consistent near infrared spectroscopic assay for biomass enzymatic digestibility upon various physical and chemical pretreatments in Miscanthus. *Bioresource Technology,* **121**, 274-281.
14. Kelley, S.S., Rowell, R.M., Davis, M., Jurich, C.K., Ibach, R. 2004. Rapid analysis of the chemical composition of agricultural fibers using near infrared spectroscopy and pyrolysis molecular beam mass spectrometry. *Biomass and Bioenergy*, **27**(1), 77-88.
15. Labbé, N., Harper, D., Rials, T. 2006. Chemical structure of wood charcoal by infrared spectroscopy and multivariate analysis. *Journal of Agricultural and Food Chemistry*, **54**(10), 3492-3497.
16. Labbé, N. Lee, S., Cho, H., Jeong, M., André, A. 2008. Enhanced discrimination and calibration of biomass NIR spectral data using non-linear kernel methods. *Bioresource Technology, **99***(17), 8445-8452.
17. Mitsui, K., Inagaki, T., Tsuchikawa, S. 2008. Monitoring of hydroxyl groups in wood during heat treatment using NIR spectroscopy. *Biomacromolecules*, **9**(1), 286-288.
18. Nkansah, K., Dawson-Andoh, B., Slahor, J. 2010. Rapid characterization of biomass using near infrared spectroscopy coupled with multivariated data analysis: Part 1 yellow-poplar (*Liriodendron tulipifera L.*). *Bioresource Technology*, **101**(12), 4570-4576.

19. Olsson, A.M., Salmen, L. 2004. The association of water to cellulose and hemicellulose in paper examined by FTIR spectroscopy. *Carbohydrate Research*, **339**(4), 813-818.
20. Phanphanich, M., Mani, S. 2011. Impact of torrefaction on the grindability and fuel characteristics of forest biomass. *Bioresource Technology*, **102**(2), 1246-1253.
21. Prins, M.J., Ptasinski, K.J., Janssen, F.J.J.G. 2006. Torrefaction of wood - Part 2. Analysis of products. *Journal of Analytical and Applied Pyrolysis*, **77**(1), 35-40.
22. Ralph, J., Hatfield, R.D. 1991. Pyrolysis-Gc-Ms Characterization of Forage Materials. *Journal of Agricultural and Food Chemistry*, **39**(8), 1426-1437.
23. Rousset, P., Aguiar, C., Labbe, N., Commandre, J.M. 2011a. Enhancing the combustible properties of bamboo by torrefaction. *Bioresource Technology*, **102**(17), 8225-8231.
24. Rousset, P., Davrieux, F., Macedo, L., Perre, P. 2011b. Characterisation of the torrefaction of beech wood using NIRS: Combined effects of temperature and duration. *Biomass and Bioenergy*, **35**(3), 1219-1226.
25. Sanderson, M.A., Agblevor, F., Collins, M., Johnson, D.K. 1996. Compositional analysis of biomass feedstocks by near infrared reflectance spectroscopy. *Biomass and Bioenergy*, **11**(5), 365-370.
26. Schwanninger, M., Hinterstoisser, B., Gierlinger, N., Wimmer, R., Hanger, J. 2004. Application of Fourier transform near infrared Spectroscopy (FT-NIR) to thermally modified wood. *Holz Als Roh-Und Werkstoff*, **62**(6), 483-485.
27. Schwanninger, M., Rodrigues, J.C., Fackler, K. 2011. A review of band assignments in near infrared spectra of wood and wood components. *Journal of near Infrared Spectroscopy*, **19**(5), 287-308.
28. Shang, L., Ahrenfeldt, J., Holm, J.K., Sanadi, A.R., Barsberg, S., Thomsen, T., Stelte, W., Henriksen, U.B. 2012. Changes of chemical and mechanical behavior of torrefied wheat straw. *Biomass and Bioenergy*, **40**, 63-70.
29. Sun, B.L., Liu, J.L., Liu, S.J., Yang, Q. 2011. Application of FT-NIR-DR and FT-IR-ATR spectroscopy to estimate the chemical composition of bamboo (Neosinocalamus affinis Keng). *Holzforschung*, **65**(5), 689-696.
30. Tjeerdsma, B.F., Militz, H. 2005. Chemical changes in hydrothermal treated wood: FTIR analysis of combined hydrothermal and dry heat-treated wood. *Holz Als Roh-Und Werkstoff*, **63**(2), 102-111.
31. Via, B.K., Fasina, O., Pan, H. 2011. Assessment of Pine Biomass Density through Mid-Infrared Spectroscopy and Multivariate Modeling. *Bioresources*, **6**(1), 807-822.
32. Wentzell, P.D., Montoto, L.V. 2003. Comparison of principal components rgression and partial least squares regression through genertic simulations of complex mixtures. *Chemometrics and Intelligent Laboratory Systems,* **65**(2), 257-279.

http://www.nrel.gov/biomass/pdfs/42622.pdf. Last accessed date: 27/09/2012.

Table Captions:

Table 1. Full factorial design utilized for torrefaction with 3 replications each or n=90 total samples.

Table 2. Physicochemical Properties of torrefied biomass on dry basis

Table 3. Summary of significant correlations between NIR and FTIR wavenumbers with the temperature and duration increases acting as the perturbation on an otherwise homogenous material.

Table 4. Summary of PCR predictions of proximate analysis from NIR and FTIR spectra

Figure Captions:

Figure 1. Two dimensional correlation contour map of the pearson correlation coefficient (r-value) between wavenumbers in the NIR and Mid IR region where areas in red represent r-values between 0.6 to 0.9 while areas in gray represent r-values between 0.4 to 0.6.

Figure 2. NIR predicted proximate analysis from PCR versus that measured from conventional methods for (a) volatiles (b) ash (c) moisture (d) higher heating value (e) fixed carbon

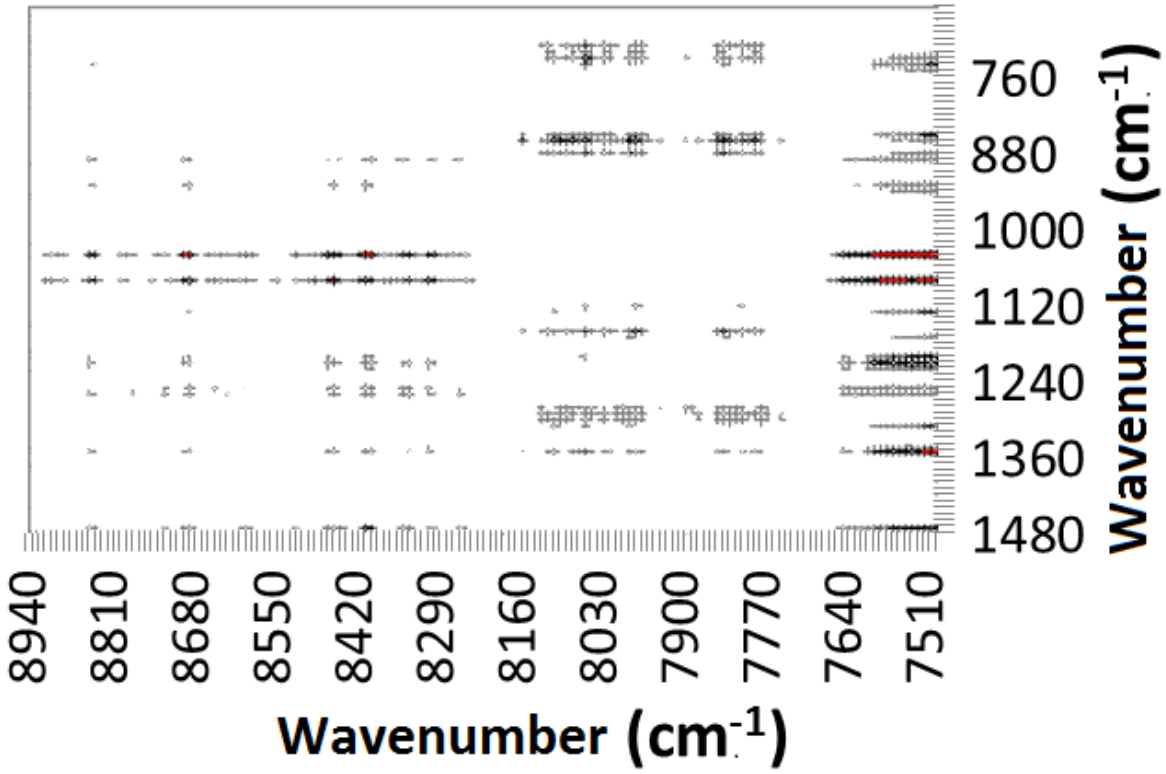
760
880
1000
1120
1240
1360
1480
Wavenumber (cm-1)
8940
8810
8680
8550
8420
8290
8160
8030
7900
7770
7640
7510
Wavenumber (cm-1)

Fig. 1

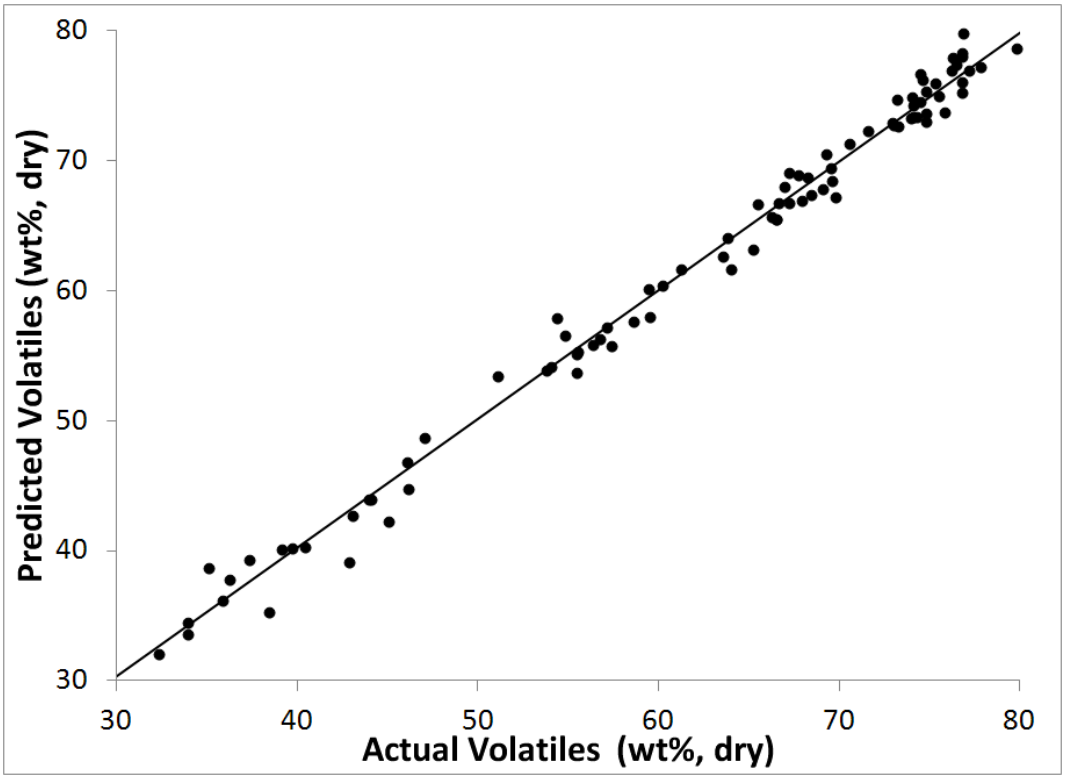
Predicted Volatiles (wt%, dry)
Actual Volatiles (wt%, dry)
30
40
50
60
70
80

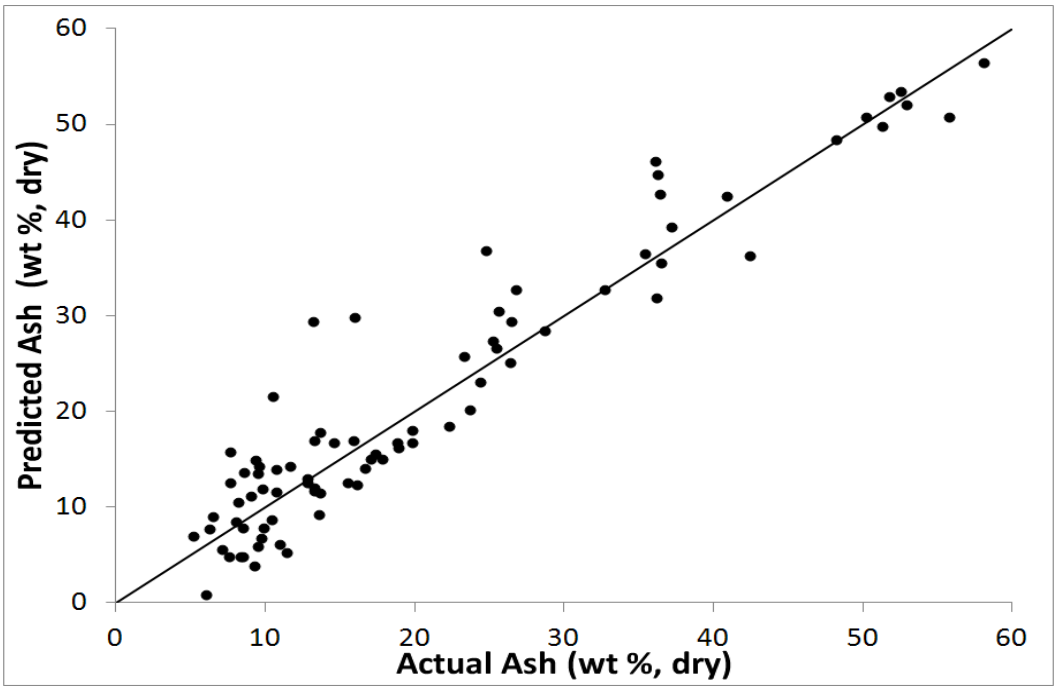
Predicted Ash (wt %, dry)
Actual Ash (wt %, dry)
0
10
20
30
40
50
60

Fig. 2 (a) (b)

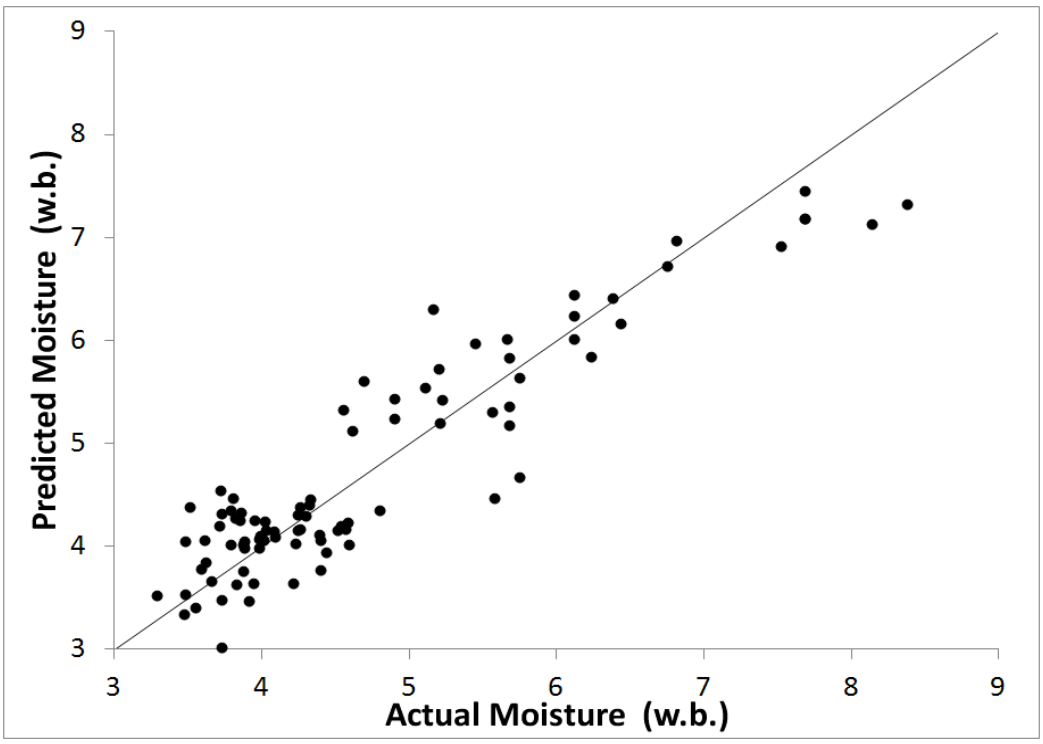
Predicted Moisture (w.b.)
Actual Moisture (w.b.)
3
4
5
6
7
8
9

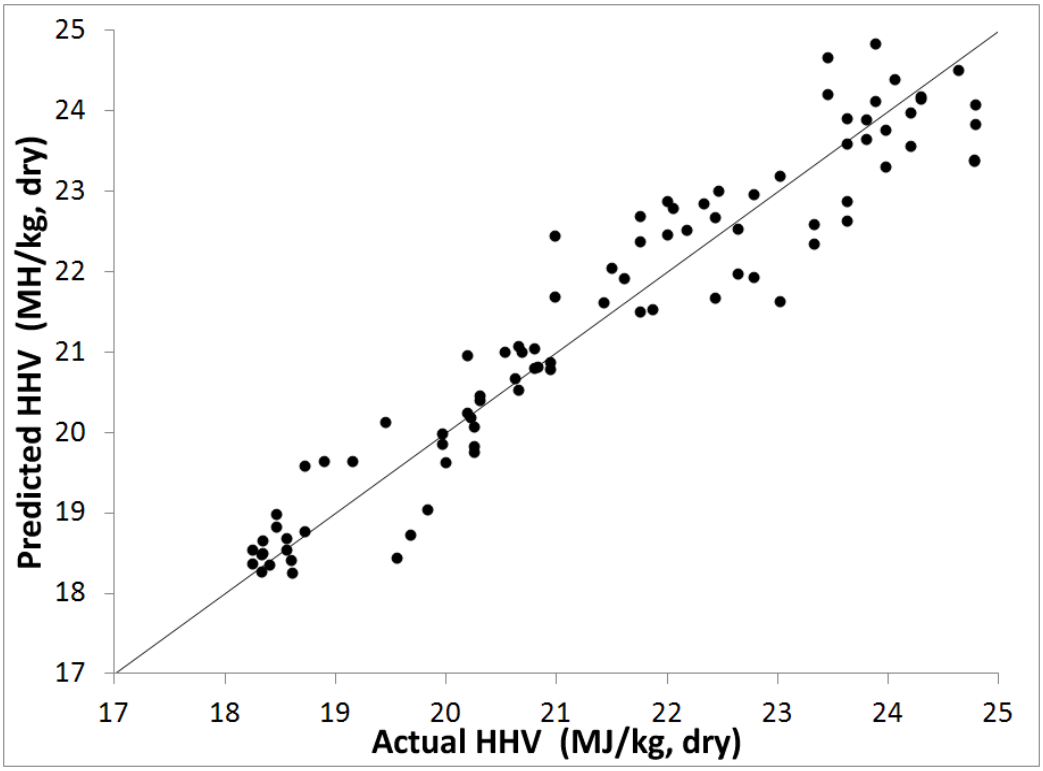
Predicted HHV (MH/kg, dry)
Actual HHV (MJ/kg, dry)
17
18
19
20
21
22
23
24
25

Fig. 2 (c) (d)

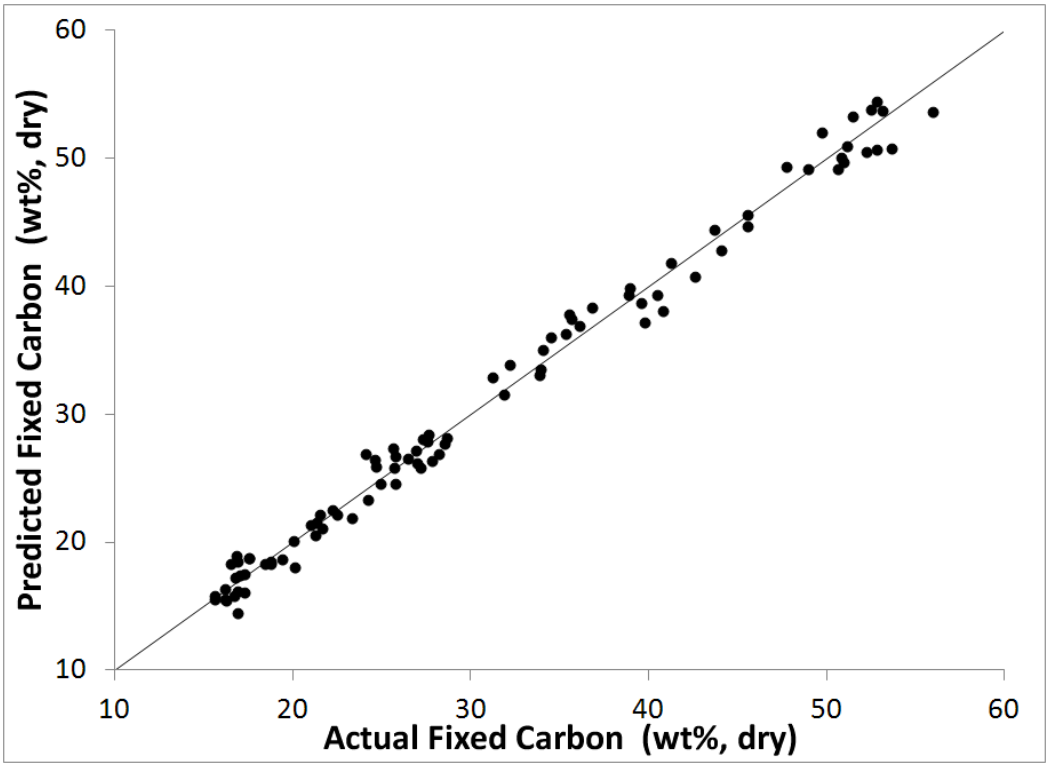
Predicted Fixed Carbon (wt%, dry)
Actual Fixed Carbon (wt%, dry)
10
20
30
40
50
60

Fig. 2 (e)

Table 1

Full factorial design utilized for torrefaction with 3 replications each or n=90 total samples.

Factor 1 - Biomass	Factor 2 - Temperature (C^{o})	Factor 3 - Duration (minutes)
Sweetgum	Room Temperature (control only)	No time duration (control only)
Pine	225	15
Switchgrass	250	30
	275	45

Table 2

Physicochemical Properties of torrefied biomass on dry basis

Sample[a]	Proximate Analysis			HHV
	Ash (wt%)	Volatiles (wt%)	Fixed Carbon (wt%)	(MJ/kg)
Pine (raw)	0.72	80.79	18.49	20.178
225-15	0.63	80.53	18.84	20.503
225-30	0.87	76.37	22.75	21.112
225-45	0.94	65.45	33.61	22.501
250-15	1.00	76.57	22.43	21.279
250-30	0.96	70.03	29.02	22.396
250-45	1.08	59.75	39.17	24.010
275-15	0.94	70.90	28.16	21.909
275-30	0.98	56.53	42.49	24.719
275-45	1.40	43.17	55.43	26.678
Sweetgum (raw)	1.39	81.41	17.20	19.649
225-15	1.09	82.24	16.66	20.426
225-30	1.35	78.43	20.22	20.910
225-45	1.65	73.27	25.08	22.461
250-15	1.46	78.40	20.15	19.918
250-30	1.87	71.54	26.59	21.609
250-45	2.18	60.02	37.80	22.672
275-15	1.79	70.87	27.34	21.574
275-30	2.53	59.64	37.84	23.369
275-45	3.08	44.27	52.65	25.860
Switchgrass (raw)	2.71	79.18	18.12	19.498

225-15	2.77	79.38	17.85	19.389
225-30	3.75	67.45	28.80	21.409
225-45	5.39	48.25	46.36	23.988
250-15	3.67	69.85	26.48	21.018
250-30	5.37	49.37	45.25	24.344
250-45	6.62	39.00	54.38	25.451
275-15	4.21	60.03	35.76	22.625
275-30	6.40	38.68	54.92	26.246
275-45	7.24	34.82	57.94	25.952

[a] The first and second numbers represent temperature and time of treatment.

Table 3

Summary of significant correlations between NIR and FTIR wavenumbers with the temperature and duration increases acting as the perturbation on an otherwise homogenous material.

NIR Band Location (cm^{-1})	NIR Band Assignment	FTIR Band Location (cm^{-1})	FTIR Band Assignment	Pearson Correlation Coefficient
7410	C-H def. + str. For CH_3 in hemicellulose	1360	Aliphatic C-H def.	0.67
6660	O-H str. in cellulose	900	C-O-H def.	0.41
6003	C-H str. in CH_3 in hemicellulose	1360	Aliphatic C-H def.	0.67
5980	C-H str. for aromatic C-H due to lignin	1035	Aromatic C-H in-plane def.	0.77
5848	C-H str. in furanose or pyranose of hemicellulose	1740	C=O stretch in hemicellulose	0.84
5464	O-H str. + C-O str. due to semi & crystalline cellulose region	1335	C-O-H deformation in cellulose	0.67
5240	Lignin in branch material	850	C-H due to aromatic structure in lignin	0.68
5220 - 5051	O-H asym str. and O-H def. in water	1600	Water	0.70
4392 - 4365	O-H str. + C-C str. & C-H str + C-H def. & C-O str. in cellulose	1730	Weak carbonyl (C=O) stretch in cellulose	0.56
4392 - 4365	Same	1280	CH_2-O-H def. in cellulose	0.81
4091	Not assigned	1515	Aromatic skeleton vibration in lignin	0.72

Table 4

Summary of PCR predictions of proximate analysis from NIR and FTIR spectra

	Moisture		Ash		Volatiles		Fixed Carbon		HHV	
	NIR	FTIR	NIR	FTIR	NIR	FTIR	NIR	FTIR	NIR	FTIR
Pretreat	Raw	Der.	Raw	Der.	Der.	Raw	Raw	Raw	Raw	Der.
R^2	0.85	0.74	0.92	0.82	0.99	0.91	0.99	0.91	0.92	0.81
Adj R^2	0.84	0.71	0.91	0.81	0.98	0.91	0.98	0.90	0.91	0.80
RMSEC	0.0048	0.0064	0.0053	0.0080	0.0173	0.0433	0.0135	0.038	0.6076	0.911
RMSEP	0.0051	0.0072	0.0056	0.0083	0.0181	0.0457	0.0143	0.041	0.6384	1.145
# Factors	5	8	8	6	7	7	7	5	5	5